

Joint Range and Angle Estimation for FMCW MIMO Radar and Its Application

Junghoon Kim, Joohwan Chun, and Sungchan Song

Abstract—Recently, frequency-modulated continuous wave (FMCW) radars with array antennas are gaining in popularity on a wide variety of commercial applications. A usual approach of the range and angle estimation of a target with an array FMCW radar is to form a range-angle matrix with deramped receive signal, and then apply the two-dimensional fast Fourier transformation (2D-FFT) on the range-angle matrix. However, such frequency estimation approaches give bias error because two frequencies on the range-angle matrix are not independent to each other, unlike the 2D angle estimation with a passive planar antenna array. We propose a new maximum-likelihood based algorithm for the joint range and angle estimation of multiple targets with an array FMCW radar, and show that the proposed algorithm achieves the Cramer-Rao bounds (CRBs) both for the range and angle estimation. The proposed algorithm is also compared with other algorithms for a simultaneous localization and mapping (SLAM) problem.

Index Terms—FMCW radars, maximum likelihood estimation, 2D-FFT, 2D-MUSIC, CRB, joint range and angle estimation

I. INTRODUCTION

Frequency-modulated continuous wave (FMCW) radars are widely used in short-range applications such as altimeters [1], automotive radars [2]–[4] and more recently, synthetic aperture radars (SARs) [5]–[9]. Advantages of FMCW radars lie in their light weight, low power consumption and cost-effectiveness, while achieving relatively high range resolution [10], [11]. FMCW radars may have a full receive (Rx) antenna array or a multiple-input multiple-output (MIMO) virtual antenna array [12]–[15]. Either with the full Rx array or with the MIMO virtual array, we first form a range-angle matrix, where the angle dimension may extend to the size of the virtual array in case of the MIMO system. Then, to get range and angle estimates of each target, we may apply two-dimensional (2D) frequency estimation algorithms on the range-angle matrix, such as the 2D fast Fourier transformation (2D-FFT) [13], joint angle-frequency estimation (JAFE) [16], 2D multiple signal classification (2D-MUSIC) [14], or the joint discrete Fourier transform (DFT)-estimation of signal parameters via rotational invariance techniques (ESPRIT) [17].

However, these traditional 2D frequency estimation algorithms ignore the fact that two frequencies on each domain are dependent on each other and are coupled. This is because the frequency on the range domain, which is proportional to the

range to the target, differs slightly at each antenna, depending on the angle to the target. Most previous works do not include the range difference per antenna in the signal model, resulting in inevitable bias error. We remark that the least squares estimation algorithm in [18] can handle the range difference of antennas, and yields an accurate estimation in case of a single target. However with multiple targets, interference from other targets degrades the performance.

We propose a maximum-likelihood algorithm for the joint range and angle estimation of multiple targets with FMCW radars, to solve the aforementioned bias and interference error problem. We also derive the Cramer-Rao bounds (CRBs) of the estimates, and compare the proposed algorithm with other algorithms as well as the CRB. We remark that the proposed algorithm is applicable not only to the range-angle domain but to the ordinary range-Doppler or to the angle-Doppler domain of the space-time adaptive processing (STAP) [19]. This is because we similarly have the range difference along the pulse dimension on the range-Doppler domain, and the angle difference along the pulse dimension on the angle-Doppler domain.

The proposed algorithm would be of benefit to the radar-based simultaneous localization and mapping (SLAM), which updates the map of unknown environment, while simultaneous keeping track of own vehicle autonomously [20], [21], for short-distance autonomous navigation. If the vehicle carries an on-board environmental map, it may use the global positioning system (GPS) receiver or its own active sensor such as radar [22] to localize itself. However, the GPS signal is not accurate enough for precision navigation, and is not even available in indoor environment. Also the map is not very useful for non-static environment such as with moving objects. To localize the own vehicle relative to the environment, the radar-based SLAM utilizes the range and angle measurements to a set of scatterers, called a point cloud, of a nearby opportunistic objects, as explained briefly below.

First, consider a vehicle that is standing at the exactly known origin. The radar in the vehicle measures the ranges and angles to the scatterers of objects nearby. These measurements will fix the position of those scatterers. When the vehicle moves to a new position after a very short period of time, relative positions of those scatterers seen from the vehicle will alter. Then by comparing the two sets of relative positions of the scatterers, before and after the movement, the vehicle is able to determine its new location. This new location becomes the new origin, and by repeating the above process the vehicle can keep track of its trajectory relative to the nearby objects. Notice that measurement error in the range and angle will accumulate

Junghoon Kim and Joohwan Chun are with Department of Electrical Engineering, Korea Advanced Institute of Science and Technology, Daejeon, South Korea and Sungchan Song, with Hanwha Systems, Yongin City, South Korea.

This work was supported in part by Hanwha Systems under the industry-academia collaboration program in 2017.

during the SLAM procedure, and therefore the final position error of the vehicle can become quite large even with small error in the range and angle estimates.

In Sec 2, we shall show that the traditional 2D frequency estimation algorithms will give bias error in the estimated range and angle. A new maximum likelihood estimation algorithm is presented in Sec 3, and its performance and comparison with other algorithms are given in Sec 4. In Sec 5, we shall show that SLAM utilizing the iterative closest point (ICP) method with the range and angle estimates provided by the proposed algorithm will be able to localize the own vehicle accurately during the autonomous valet parking procedure [23]–[25], which is a special case of SLAM. Conclusions are made in Sec 6.

II. ESTIMATION ERROR OF CONVENTIONAL APPROACHES

A. FMCW radar signal model

The received deramped FMCW radar signal at a single antenna, for a single target, at time n is given by

$$s[n] = ae^{j\phi} e^{j(2\pi\gamma\tau T_s n + 2\pi f_c \tau - \pi\gamma\tau^2)}, \quad 0 \leq n \leq N-1, \quad (1)$$

where $ae^{j\phi}$ is the reflectivity of the target, f_c is the operating frequency, γ is the chirp rate, T_s is the sampling period, τ is the time delay from the target to the receive antenna, and N is the total number of samples.

Let us assume that there are $M = PQ$ virtual receive antennas, where P and Q are the numbers of transmit and receive antennas, respectively, and that the array is uniform and linear with the inter-antenna spacing of $d = \lambda/2$, where $\lambda = c/f_c$ is the wavelength of the signal. Further, assuming that there are K targets, let us denote the incident angle of the signal from the k th target, $1 \leq k \leq K$ by θ_k , and the distance from the origin to the target, by r_k . Then the time delay $\tau_k[m]$ to the m th antenna, $0 \leq m \leq M-1$ from the k th target will be

$$\tau_k[m] = (2r_k + mu_k)/c, \quad u_k = d \sin \theta_k, \quad (2)$$

where c is the speed of light and u_k is the signal path-length difference between two adjacent antennas.

Therefore, the deramped signal at the m th antenna, reflected from the k th target will be

$$s_k[n, m] = a_k e^{j(\phi_k - \pi\gamma\tau_k^2[m])} e^{j(2\pi f_c \tau_k[m] + 2\pi\gamma\tau_k[m]T_s n)} \quad (3)$$

$$= a_k e^{j(\phi_k - \pi\gamma\tau_k^2[m] + 4\pi f_c r_k/c)} \times e^{j2\pi f_c m u_k/c} e^{j2\pi\gamma(2r_k + m u_k)/c T_s n} \quad (4)$$

$$\approx a_k e^{j\psi_k} e^{j2\pi \frac{u_k}{\lambda} m} e^{j2\pi(2r_k + m u_k) \frac{B}{cN} n}, \quad (5)$$

where in (5) we have used the relationship between the chirp rate γ and the bandwidth of the signal B ; $\gamma = B/(NT_s)$ and the approximation that $\pi\gamma\tau_k^2[m]$ is not dependent on m , resulting in

$$\psi_k \approx \phi_k - \pi\gamma\tau_k^2[m] + 4\pi f_c r_k/c. \quad (6)$$

Now the measurement at time n and at antenna m is the noisy sum of the signals from all targets,

$$z[n, m] = \sum_{k=1}^K s_k[n, m] + w[n, m], \quad (7)$$

where $w[n, m] \sim CN(0, \sigma^2)$ is complex additive Gaussian noise.

B. Bias error in the two-dimensional frequency estimation algorithms

Two-dimensional frequency estimation algorithms, such as 2D-FFT [13] and 2D-MUSIC [14] may be applied to get the range and angle estimates from the measurement (7). We shall show that such methods always give bias error for both range and angle estimates, even with noiseless measurement and under infinite number of zero-padding, i.e., under the discrete-time Fourier transformation (DTFT).

Let us consider the measurement (7) under noiseless condition for a single target, with the definition of $y_\theta = Mu/\lambda = (M \sin \theta)/2$, $x_r = 2Br/c$, and $x_\theta = Bu/c = (B \sin \theta)/(2f_c)$. Then

$$z[n, m] = ae^{j\psi} e^{j2\pi \frac{u}{\lambda} m} e^{j2\pi(2r + mu) \frac{B}{cN} n} \quad (8)$$

$$= ae^{j\psi} e^{j2\pi \frac{y_\theta}{M} m} e^{j2\pi \frac{x_r + m x_\theta}{N} n}. \quad (9)$$

In the below, it will be shown that the coupling term x_θ , presenting in the measurement is responsible for the bias of the estimate. Let us consider the DTFT,

$$S(x, y) = \sum_{n=0}^{N-1} \sum_{m=0}^{M-1} z[n, m] e^{-j2\pi \frac{x}{N} n} e^{-j2\pi \frac{y}{M} m}. \quad (10)$$

Our goal is to determine $(x', y') = \arg \max |S(x, y)|$, and then, using $x' = 2Br'/c$ and $y' = M \sin \theta'/2$, compute r' and θ' , which are to be compared with the true r and θ . Notice that

$$|S(x', y')| = a \left| \sum_{n=0}^{N-1} \sum_{m=0}^{M-1} e^{j2\pi \frac{(x_r + m x_\theta - x')}{N} n} e^{j2\pi \frac{y_\theta - y'}{M} m} \right| \quad (11)$$

$$= a \left| \sum_{m=0}^{M-1} \frac{\sin(\pi(x_r + m x_\theta - x')/N)}{\sin(\pi(x_r + m x_\theta - x')/N)} \right| \quad (12)$$

$$\times e^{j\pi \frac{N-1}{N} (x_r + m x_\theta - x')} e^{j2\pi \frac{y_\theta - y'}{M} m} \left| \right. \\ = a \left| \sum_{m=0}^{M-1} \frac{\sin(\pi(x_r + m x_\theta - x')/N)}{\sin(\pi(x_r + m x_\theta - x')/N)} e^{j\pi \frac{N-1}{N} m x_\theta} e^{j2\pi \frac{y_\theta - y'}{M} m} \right|. \quad (13)$$

The first factor in (13) can be simplified further by using the following inequalities, which are proven in the sequel,

$$\frac{\pi}{N} \max_m |x_r + m x_\theta - x'| \leq \frac{\pi}{N} (M-1) |x_\theta| \quad (14)$$

$$\leq \frac{\pi}{N} (M-1) \frac{B}{2f_c} \quad (15)$$

$$\ll 1. \quad (16)$$

We know x' must be close to the true value x_r , and therefore $x' \in [x_r, x_r + (M-1)x_\theta]$ when $x_\theta \geq 0$, or $x' \in [x_r + (M-1)x_\theta, x_r]$ when $x_\theta < 0$, which assures the inequality (14). In addition, $N \gg M$ and $f_c \gg B$ hold commonly, which makes

the inequality (16) valid. Therefore, using $(N-1)/N \approx 1$ in addition, (13) can be approximated as

$$|S(x', y')| \approx aN \left| \sum_{m=0}^{M-1} \frac{\sin(\pi(x_r + mx_\theta - x'))}{\pi(x_r + mx_\theta - x')} e^{j\pi mx_\theta} e^{j2\pi \frac{y_\theta - y'}{M} m} \right| \quad (17)$$

$$= aN \left| \sum_{m=0}^{M-1} \text{sinc}(x_r + mx_\theta - x') e^{j2\pi \frac{y_\theta + Mx_\theta/2 - y'}{M} m} \right|. \quad (18)$$

Furthermore, if $(M-1)B/(2f_c) < 1$, which is mostly the case, then we have $\max_m |x_r + mx_\theta - x'| < 1$ from (15), which leads $\text{sinc}(x_r + mx_\theta - x') > 0$. Therefore (18) becomes the maximum when the exponent of the complex exponential function is zero, i.e.,

$$y' = y_\theta + \frac{M}{2} x_\theta. \quad (19)$$

Now by inserting $y' = (M \sin \theta')/2$, $y_\theta = (M \sin \theta)/2$, and $x_\theta = (B \sin \theta)/(2f_c)$ into (19), we get

$$\theta' = \sin^{-1} \left(\left(1 + \frac{B}{2f_c}\right) \sin \theta \right). \quad (20)$$

With this y' in (19), (18) reduces to

$$|S(x', y')| = aN \left| \sum_{m=0}^{M-1} \text{sinc}(x_r + mx_\theta - x') \right|. \quad (21)$$

Noting that $\text{sinc}(x_r + mx_\theta - x') > 0$, (21) will be the maximum when all M points of $\text{sinc}(x_r + mx_\theta - x')$ for $0 \leq m \leq M-1$, are symmetrically placed around the peak. Therefore

$$x' = x_r + \frac{M-1}{2} x_\theta. \quad (22)$$

By inserting $x' = 2Br'/c$, $x_r = 2Br/c$, and $x_\theta = (B \sin \theta)/(2f_c)$ into (22), we get

$$r' = r + \frac{(M-1)}{8} \lambda \sin \theta. \quad (23)$$

Finally, from (20) and (23), the bias errors of the angle and range estimates are given by

$$r^{(b)} = r' - r = \frac{(M-1)\lambda}{8} \sin \theta, \quad (24)$$

$$\theta^{(b)} = \theta' - \theta = \sin^{-1} \left(\left(1 + \frac{B}{2f_c}\right) \sin \theta \right) - \theta. \quad (25)$$

C. The least square estimation algorithm

Feger et al. have proposed a least squares estimation (LSE) algorithm that maximizes the function $J(r, u)$, using a localized grid-search [18]. The function $J(r, u)$ is essentially identical to $|S(x, y)|$ in (10) after the change of variables. This LSE algorithm gives good estimation performance for a single target, because it retains the range-angle coupling term. However for a target with a completely unknown position, a full grid search is needed with high computational cost. Also, when multiple targets present, the interference between targets causes error on the range and angle estimates.

III. PROPOSED ESTIMATION ALGORITHM

The objective is to find the maximum likelihood estimates of ψ_k , a_k , u_k and r_k , where ψ_k and a_k are nuisance parameters. Let us first rewrite the signal (5) as

$$s_k[n, m] = a_k e^{j\psi_k} e^{j2\pi \frac{u_k}{\lambda} m} g_k[n, m], \quad (26)$$

where $g_k[n, m] = e^{j2\pi(2r_k + mu_k) \frac{B}{cN} n}$. We stack the time samples of measurement (7) into a column vector $\mathbf{z}^{(m)} \in \mathbb{C}^{N \times 1}$, as below.

$$\mathbf{z}^{(m)} = \sum_{k=1}^K \mathbf{s}_{(k)}^{(m)} + \mathbf{w}^{(m)}, \quad (27)$$

where

$$\mathbf{s}_{(k)}^{(m)} = a_k e^{j\psi_k} e^{j2\pi \frac{u_k}{\lambda} m} \mathbf{g}_{(k)}^{(m)}, \quad (28)$$

$$\mathbf{g}_{(k)}^{(m)} = [g_k[0, m], g_k[1, m], \dots, g_k[N-1, m]]^T, \quad (29)$$

$$\mathbf{w}^{(m)} = [w[0, m], w[1, m], \dots, w[N-1, m]]^T. \quad (30)$$

Then, the likelihood function is

$$\Lambda_0 = \sum_{m=0}^{M-1} \left[\mathbf{z}^{(m)} - \sum_{k=1}^K \mathbf{s}_{(k)}^{(m)} \right]^H \cdot \frac{1}{\sigma^2} I \cdot \left[\mathbf{z}^{(m)} - \sum_{k=1}^K \mathbf{s}_{(k)}^{(m)} \right] \quad (31)$$

$$\begin{aligned} &= \frac{1}{\sigma^2} \sum_{m=0}^{M-1} \left[\mathbf{z}^{(m)H} \cdot \mathbf{z}^{(m)} \right] \\ &\quad - \frac{1}{\sigma^2} \sum_{m=0}^{M-1} \left[\mathbf{z}^{(m)H} \cdot \sum_{k=1}^K \mathbf{s}_{(k)}^{(m)} + \left(\sum_{k=1}^K \mathbf{s}_{(k)}^{(m)} \right)^H \cdot \mathbf{z}^{(m)} \right] \\ &\quad + \frac{1}{\sigma^2} \sum_{m=0}^{M-1} \left[\left(\sum_{k=1}^K \mathbf{s}_{(k)}^{(m)} \right)^H \cdot \sum_{k=1}^K \mathbf{s}_{(k)}^{(m)} \right], \end{aligned} \quad (32)$$

where the superscript H denotes the conjugated transposition. After inserting (28) into (32) and removing unnecessary terms, the likelihood function becomes

$$\begin{aligned} &\Lambda(a_1, \psi_1, r_1, u_1, \dots, a_K, \psi_K, r_K, u_K) \\ &= - \sum_{m=0}^{M-1} \sum_{k=1}^K a_k \left[e^{j(\psi_k + 2\pi \frac{u_k}{\lambda} m)} R_{(k)}^{(m)} + e^{-j(\psi_k + 2\pi \frac{u_k}{\lambda} m)} R_{(k)}^{(m)*} \right] \\ &\quad + \sum_{m=0}^{M-1} \sum_{k=1}^K \sum_{l \neq k}^K a_k a_l e^{j(\psi_k + 2\pi \frac{u_k}{\lambda} m)} e^{-j(\psi_l + 2\pi \frac{u_l}{\lambda} m)} R_{(l,k)}^{(m)} \\ &\quad + MN \sum_{k=1}^K a_k^2, \end{aligned} \quad (33)$$

where

$$R_{(k)}^{(m)} = \mathbf{z}^{(m)H} \cdot \mathbf{g}_{(k)}^{(m)} = \sum_{n=0}^{N-1} z^*[n, m] e^{j2\pi(2r_k + mu_k) \frac{B}{cN} n}, \quad (34)$$

$$R_{(l,k)}^{(m)} = \mathbf{g}_{(l)}^{(m)H} \cdot \mathbf{g}_{(k)}^{(m)} = \sum_{n=0}^{N-1} e^{j2\pi(2r_k + mu_k - 2r_l - mu_l) \frac{B}{cN} n}. \quad (35)$$

Here, $R_{(l,k)}^{(m)}$ represents interferences from other targets, and retaining this term allows the proposed algorithm to achieve the CRB, even in multiple target environment.

The parameters, ψ_k , a_k , u_k , and r_k can be found by maximizing $\Lambda(\cdot)$ in (33). Because $\Lambda(\cdot)$ is nonlinear, however, u_k , r_k and some other intermediate parameters needed for ψ_k ,

a_k should be found by Newton-Raphson iterations. Detailed derivations for the formulas below are given in Appendix A.

First, we determine $\hat{\psi}_k$ for all k by

$$\hat{\psi}_k = -\angle\left(\sum_{m=0}^{M-1} e^{j2\pi\frac{u_k}{\lambda}m} S_{(k)}^{(m)}\right), \quad (36)$$

where $S_{(k)}^{(m)} = R_{(k)}^{(m)} - \sum_{l \neq k}^K a_l e^{-j(\psi_l + 2\pi\frac{u_l}{\lambda}m)} R_{(l,k)}^{(m)}$, and $\angle(\cdot)$ denotes the phase of (\cdot) . See Appendix A.1.

Second, \hat{a}_k for all k are found by solving the linear system of equations,

$$\mathbf{B} \cdot \mathbf{a} = \mathbf{y}, \quad \mathbf{B} \in \mathbb{R}^{K \times K}, \quad \mathbf{y} \in \mathbb{R}^{K \times 1}, \quad (37)$$

where $\mathbf{a} = [\hat{a}_1, \dots, \hat{a}_K]^T \in \mathbb{R}^{K \times 1}$, and

$$\mathbf{B}(k, k) = MN, \quad 1 \leq k \leq K, \quad (38)$$

$$\mathbf{B}(k, l) = \sum_{m=0}^{M-1} \text{Re}[e^{j(\psi_k + 2\pi\frac{u_k}{\lambda}m)} e^{-j(\psi_l + 2\pi\frac{u_l}{\lambda}m)} R_{(l,k)}^{(m)}], \quad (39)$$

$$1 \leq k, l \leq K, \quad k \neq l,$$

$$\mathbf{y}(k) = \sum_{m=0}^{M-1} \text{Re}[e^{j(\psi_k + 2\pi\frac{u_k}{\lambda}m)} R_{(k)}^{(m)}], \quad 1 \leq k \leq K. \quad (40)$$

See Appendix A.2.

Third, \hat{u}_k for all k are determined iteratively as

$$\hat{u}_k(i+1) = \hat{u}_k(i) - \frac{f_u}{f'_u} \Big|_{\hat{u}_k = \hat{u}_k(i)}, \quad (41)$$

where $\hat{u}_k(i)$ denotes \hat{u}_k at the i th iteration, and f_u, f'_u are derived in Appendix A.3.

Fourth, we determine \hat{r}_k iteratively as

$$\hat{r}_k(i+1) = \hat{r}_k(i) - \frac{f_r}{f'_r} \Big|_{\hat{r}_k = \hat{r}_k(i)}, \quad (42)$$

where $\hat{r}_k(i)$ denotes \hat{r}_k at the i th iteration, and f_r, f'_r are derived in Appendix A.4.

The proposed joint range and angle estimation algorithm, including the initialization and termination, is summarized as Algorithm 1.

Algorithm 1 Algorithm for joint range and angle estimation

Initialization:

- 1: Determine $u_k(0)$ and $r_k(0)$ by $N \times M$ grid search on $|S(x', y')|$.
- 2: Determine $\psi_k(0) = -\angle\left(\sum_{m=0}^{M-1} e^{j2\pi\frac{u_k}{\lambda}m} R_{(k)}^{(m)}\right)$ using (34).
- 3: Determine $a_k(0)$ by solving (37).

Iteration:

- 1: $i = 0$;
 - 2: **repeat**
 - 3: Compute $R_{(k)}^{(m)}, R_{(l,k)}^{(m)}, S_{(k)}^{(m)}, \frac{\partial S_{(k)}^{(m)}}{\partial u_k}, \frac{\partial^2 S_{(k)}^{(m)}}{\partial u_k^2}, \frac{\partial S_{(k)}^{(m)}}{\partial r_k}, \frac{\partial^2 S_{(k)}^{(m)}}{\partial r_k^2}$ using $u_k(i)$ and $r_k(i)$
 - 4: Update $\psi_k(i+1), a_k(i+1), u_k(i+1)$, and $r_k(i+1)$ for all k
 - 5: $i = i + 1$
 - 6: **until** $|\Lambda(i) - \Lambda(i-1)| < \delta$
-

IV. PERFORMANCE ANALYSIS

For simulation study, the chosen operating frequency, bandwidth and the sweep time are, respectively, $f_c = 77$ GHz, $B = 4$ GHz, and $S = 10^{-4}$ s, so that the true range resolution is $\Delta r = c/(2B) = 3.75$ cm. FMCW radar chips of similar specifications are now appearing in the commercial market. In addition, the number of range samples, number of transmitting antennas and number of receive antennas are assumed to be $N = 256, P = 4$, and $Q = 4$, respectively, so that the number of virtual receive antennas is $M = PQ = 16$.

We apply a large amount of zero-padding for the 2D-FFT, and an extremely fine search, for the 2D-MUSIC and LSE, by the factor of 2048, both to the range and angle dimension. This will ensure that the grid-based algorithms; 2D-FFT, 2D-MUSIC and LSE are fairly compared with the proposed gridless algorithm, even though the computational cost of this zero-padding is prohibitively high. With this oversampling, the apparent range and angle resolutions are, respectively $\Delta r/2048 = 1.83 \times 10^{-5}$ m and $\Delta\theta/2048 = \Delta u/(du/d\theta)/2048 = 2/(M \times \cos(15^\circ)) \times 180/\pi/2048 = 0.0036^\circ$, where the angle resolution is calculated at $\theta = 15^\circ$ on which the target is assumed to be located. If the root-mean squared errors (RMSEs) of these grid-based algorithms are larger than the half of the apparent resolution, which are 9.15×10^{-6} m for the range, and 0.0018° for the angle, then the error is not caused by the lack of resolution, but by the bias of these grid-based algorithms.

A. Single target

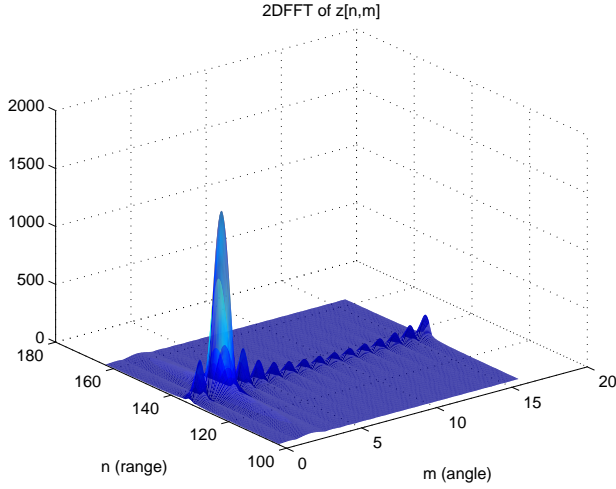
A target is assumed to be located at $r = 5$ m, and $\theta = 15^\circ$. Then the true range bin index and the true angle bin index, allowing fractions are, respectively $n_r = r/\Delta r = 133.333$, and $m_\theta = M/2 \times \sin(15^\circ) = 2.071$.

Fig. 1 shows the spectra of the 2D-FFT and 2D-MUSIC with noiseless $z[n, m]$, where the 2D-MUSIC exploits the spatial smoothing with a 10×10 sub-matrix [14]. For both 2D-FFT and 2D-MUSIC, the peak bin indices are $n_p = 133.383$ and $m_p = 2.124$, and therefore corresponding range and angle estimates are respectively, 5.00186 m and 15.397° . The bias errors of these estimates are 0.00186 m and 0.397° , which are almost the same to the theoretical values, $\Delta r^{(b)} = 0.0019$ m and $\Delta\theta^{(b)} = 0.399^\circ$ obtained from (24) and (25).

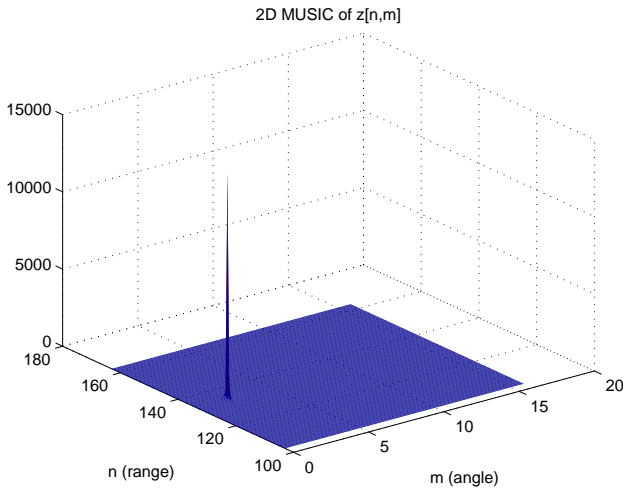
Fig. 2 shows the RMSEs of range and angle estimates against signal to noise ratio (SNR) defined as Pa^2/σ^2 . The simulation is a results of 300 trials using uniformly distributed $\psi \sim U(0, 2\pi)$. Note that both for 2D-FFT and 2D-MUSIC, the RMSEs are much larger than the apparent resolution, 1.83×10^{-5} m and 0.0036° , and therefore the errors are the bias errors, not the resolution errors. On the other hand, the LSE and the proposed algorithm give the RMSEs which coincide with the CRBs. The CRB is derived in Appendix B.

B. Multiple targets ($K = 2$)

In addition to the target at $r_1 = 5$ m and $\theta_1 = 15^\circ$, we add another target at $r_2 = 5$ m and $\theta_2 = -15^\circ$. The true range bin indices of the two targets are the same, $n_{r1} = n_{r2} =$



(a)

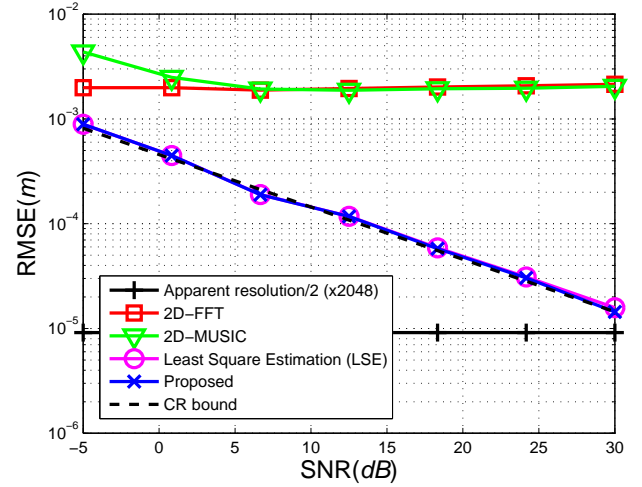


(b)

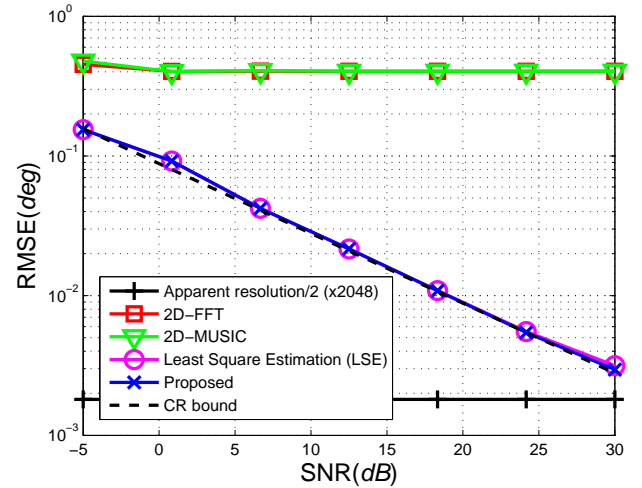
Fig. 1: The 2D frequency estimation algorithm applied to the noiseless measurement of a single target gives bias error both in the range and angle. (a) 2D-FFT spectrum. (b) 2D-MUSIC spectrum using the spatial smoothing with a 10×10 sub-matrix.

$r_1/\Delta r = 133.333$, while the true angle bin indices are $m_{\theta_1} = M/2 \times \sin(15^\circ) = 2.071$ and $m_{\theta_2} = M/2 \times \sin(-15^\circ) + M = 13.929$.

Fig. 3 shows the 2D-FFT, 2D-MUSIC spectra and the LSE function, $J(r, u)$ at the intersection of $r = 5$ m, all for noiseless $z[n, m]$. In Fig. 3(a), the indices $[n_p, m_p]$ of the two peaks are $[133.383, 2.131]$ and $[133.383, 13.869]$, which correspond to the range and angle estimates of $[5.00186$ m, $15.448^\circ]$ and $[5.00186$ m, $-15.448^\circ]$, respectively. The errors 0.00186 m and 0.448° come from two sources, the bias error given in (24) and (25), and the interference error between the two target responses. In Fig. 3(b), the indices of the peaks are $[133.383, 2.131]$ and $[133.383, 13.876]$, which give the range and angle estimates, $[5.00186$ m, $15.449^\circ]$ and $[5.00186$ m, $-15.397^\circ]$, respectively. As with the 2D-FFT case, the errors



(a)



(b)

Fig. 2: RMSEs for the single target. (a) The range estimates. (b) The angle estimates.

0.00186 m and 0.449° of the first target (and 0.00185 m and 0.397° for the second target) are a sum of the bias error and the interference error. In Fig. 3(c), the LSE function $J(r, u)$ is plotted against θ , at the fixed $r = 5$ m. Note that the peaks occur at 15.28° and -15.28° , while true angles are $\theta_1 = 15^\circ$ and $\theta_2 = -15^\circ$. This large error is caused by the sidelobe of each other.

In Fig. 4, the RMSE of the range estimate and the RMSE of the angle estimate for the first target are depicted against the SNR. Those plots for the second target are almost identical to the first target, and are omitted to conserve space. With the 2D-FFT algorithm, the range and angle estimation errors are 0.0019 m and 0.45° , respectively for both targets. With the 2D-MUSIC approach, the estimates give errors of 0.0019 m and 0.4° for both targets. Note that the proposed algorithm, which does not have bias or interference errors, achieves the CRB, while the other three grid-based algorithms, 2D-FFT, 2D-MUSIC and LSE do not.

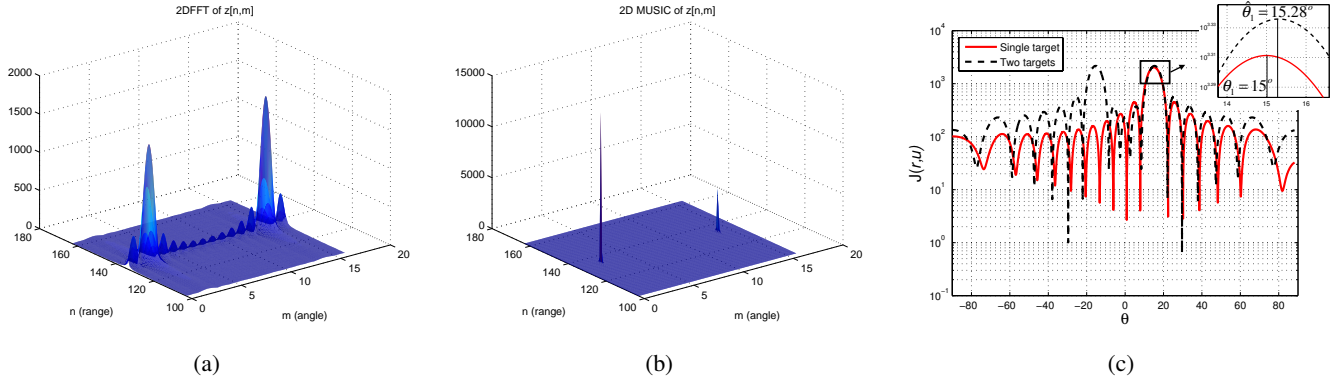


Fig. 3: For noiseless measurement of two targets, the 2D-FFT and 2D-MUSIC algorithms give bias error plus interference error, while the LSE algorithm gives interference error (a) The 2D-FFT spectrum. (b) The 2D-MUSIC spectrum using spatial smoothing with a 10×10 sub-matrix. (c) The LSE function, $J(r, u)$ at $r = 5\text{m}$.

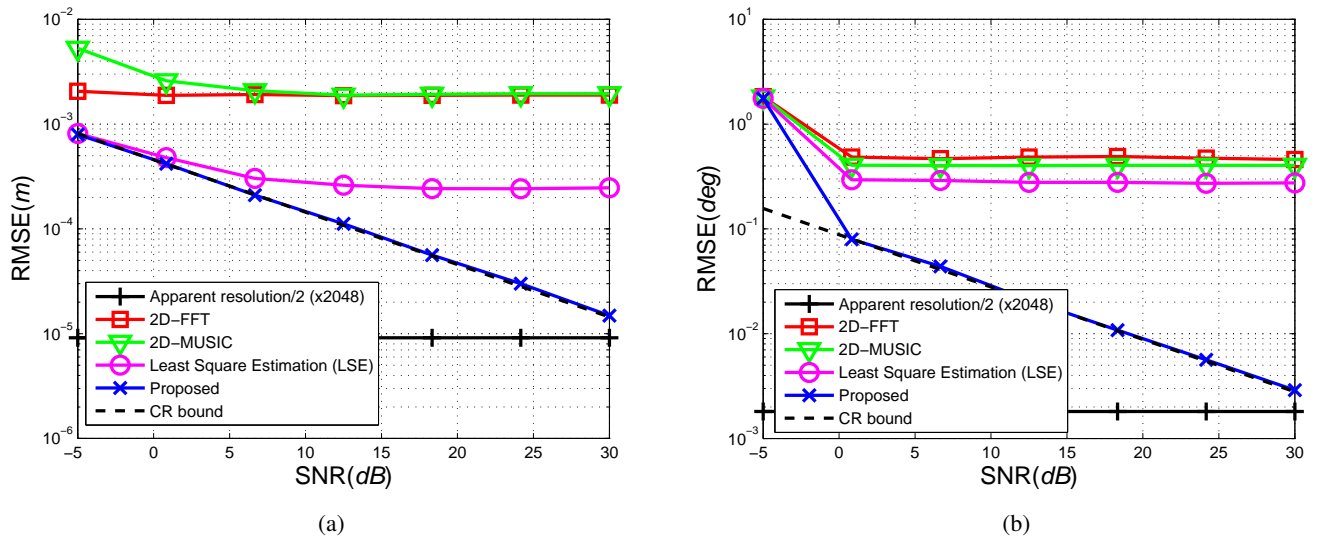


Fig. 4: RMSEs for the multiple targets. (a) The range estimates for the first target. (b) The angle estimates for the first target. The plots for the second target are almost identical to the first target.

V. APPLICATION TO THE AUTONOMOUS VALET PARKING

A. Estimation error in the scatterer positions

Fig. 5(a) shows three vehicles modeled as 2D rectangles; two vehicles are parked and the other one is about to back into the slot in-between. It is assumed that the size of the vehicle is 1.8 m wide and 4.6 m long, and that the back-parking vehicle is equipped with three radars, one on the rear and two on each side. Each radar has 4×4 MIMO antennas of 120° field of views (FOVs), constituting a virtual array of sixteen antennas. It is also assumed that two parked vehicles give rise to 66 scatterers total, which are marked with circles. Fig. 5(b) shows an enlarged view of the upper-left boxed area of Fig. 5(a). It is apparent that the proposed algorithm gives more accurate estimates than the other three algorithms. This is indeed the case as can be seen in TABLE I, which shows the RMSEs of the range, angle and the position estimates of the scatterers, averaged over 61 detected scatterers out of 66 scatterers. Notice that the estimates of the proposed algorithm are better than the other three, by an order of magnitude.

B. Localization of the vehicle

The range and angle estimates of the scatterers can be used to estimate the position and the orientation angle of the moving own-vehicle, which carries the radars, using the ICP method [26] as explained below. In Fig 6, the ground coordinate system is denoted by $x_G - y_G$ axes and the vehicle coordinate system, by $x_V - y_V$ axes. Given angle and range estimates to the scatterers, we first determine the positions of the scatterers (in the vehicle coordinate system). Let us define two point sets, $S(i) = \{\mathbf{x}_k | 1 \leq k \leq K\}$ and $S(i+1) = \{\mathbf{z}_l | 1 \leq l \leq L\}$, where $\mathbf{x}_k \in \mathbb{R}^{2 \times 1}$ and $\mathbf{z}_l \in \mathbb{R}^{2 \times 1}$ denote, respectively the positions of the scatterers in vehicle coordinates at the measurement of frame times i and $i+1$. Note that the number of scatterers may vary at every frame.

Let $\Delta \mathbf{X}_G = \mathbf{X}_G(i+1) - \mathbf{X}_G(i)$ and $\Delta \psi = \psi(i+1) - \psi(i)$ be, respectively the changes of the position and angle of the vehicle in the ground coordinate system, between frames i and $i+1$. This vehicle motion will induce the corresponding changes in the position vector and the angle of the scatterer

TABLE I: Comparison of the RMSE for the position estimates in Fig 5.

	2D-FFT	2D-MUSIC	LSE	Proposed
RMSE of the range (m)	0.0047	0.017	0.0019	0.0006
RMSE of the angle ($^\circ$)	1.30	1.99	0.40	0.13
RMSE of the 2D position (m)	0.070	0.116	0.025	0.008

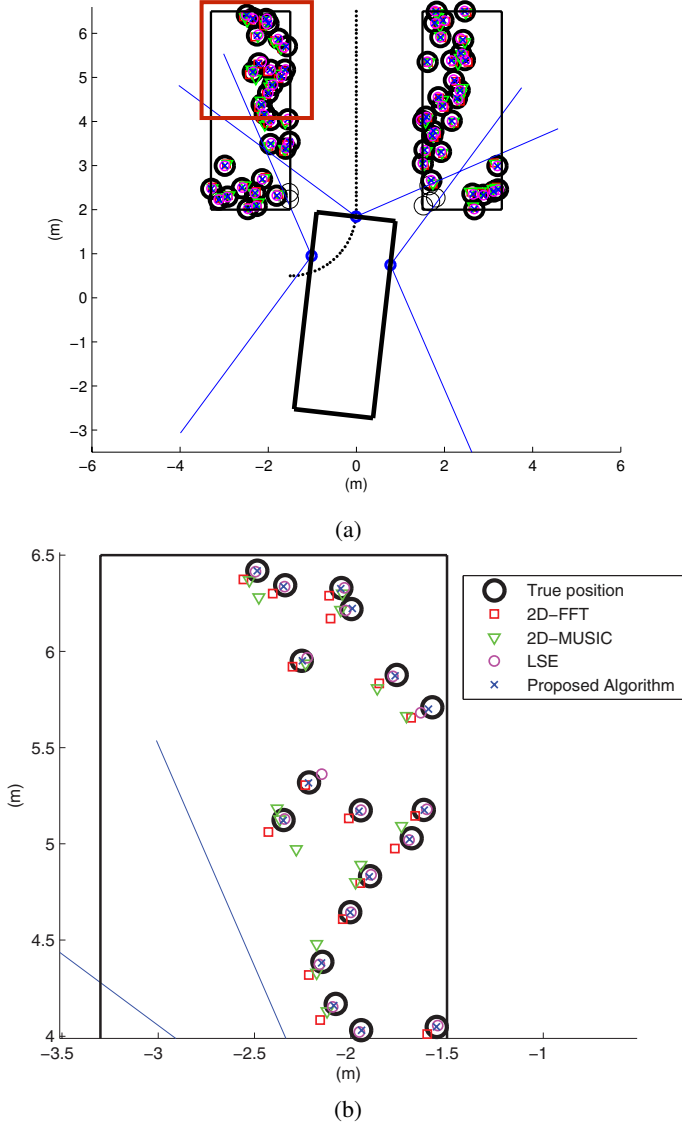


Fig. 5: (a) The vehicle in the middle has three FMCW MIMO radars, which estimate the positions of the scatterers. All three vehicles are stationary. (b) An enlarged view of the boxed area in (a).

in the vehicle coordinate system, $\Delta \mathbf{X}_V$ and $\Delta \theta$.

If we have established the association between the scatterers $\mathbf{x}_k \in S(i)$ and $\mathbf{z}_k \in S(i+1)$, $1 \leq k \leq K$, then we can find $\Delta \theta$ and $\Delta \mathbf{X}_V$ by

$$(\Delta \theta, \Delta \mathbf{X}_V) = \arg \min_{\Delta \theta, \Delta \mathbf{X}_V} \sum_{k=1}^K \|(\mathbf{z}_k - \Delta \mathbf{X}_V) - \mathbf{R}(\Delta \theta) \mathbf{x}_k\|^2, \quad (43)$$

where

$$\mathbf{R}(\Delta \theta) = \begin{bmatrix} \cos \Delta \theta & -\sin \Delta \theta \\ \sin \Delta \theta & \cos \Delta \theta \end{bmatrix}. \quad (44)$$

On the other hand, If we know $\Delta \theta$ and $\Delta \mathbf{X}_V$, then we can find the association between \mathbf{x}_k and \mathbf{z}_k by

$$\mathbf{z}_k = \arg \min_{\mathbf{z}_l \in S(i+1)} \|(\mathbf{z}_l - \Delta \mathbf{X}_V) - \mathbf{R}(\Delta \theta) \mathbf{x}_k\|^2. \quad (45)$$

However, if $\Delta \mathbf{X}_V$, $\Delta \theta$ and the association are all unknown, the above two equations (43) and (45) need to be iterated until they converge. This is one of the simplest forms of the ICP method, which is proven to converge to a local minimum [26]. With the converged $\Delta \mathbf{X}_V$ and $\Delta \theta$, the ground coordinate $\Delta \mathbf{X}_G$ and $\Delta \psi$ can be found by

$$\Delta \psi = -\Delta \theta, \quad \Delta \mathbf{X}_G = \mathbf{R}(\psi(i+1) - \pi/2) \cdot (-\Delta \mathbf{X}_V), \quad (46)$$

and the position of the vehicle can be updated as $\mathbf{X}_G(i+1) = \mathbf{X}_G(i) + \Delta \mathbf{X}_G$.

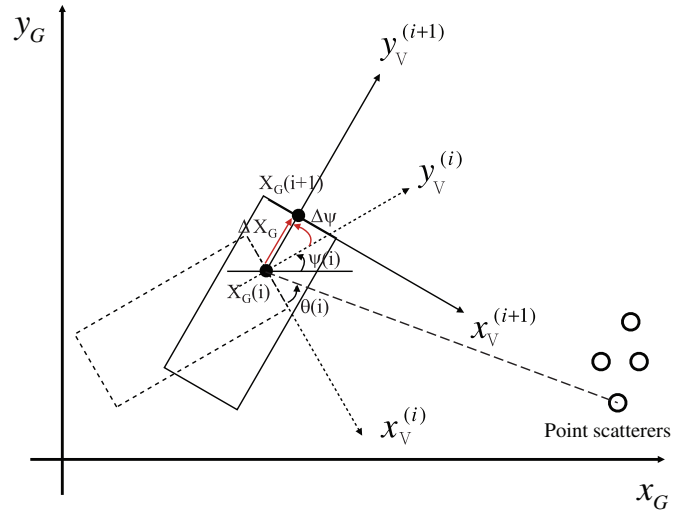


Fig. 6: Geometry of the ground coordinate system and the vehicle coordinate systems at time i and $i+1$.

C. Estimation error in the vehicle localization

The vehicle motion is modeled as a closed-loop second-order system including a damping effect and proportional-integral-derivative (PID) controller, where the vehicle mass and the damping coefficient are assumed to be 1000 kg and 50 N·s/m, respectively. The control errors in the velocity and orientation angle are zero-mean Gaussian with $N(0, 0.1 \text{ m/s})$ and $N(0, 0.1^\circ)$, respectively. The desired reference velocity is 7 km/h ($= 1.95 \text{ m/s}$) and the frame interval, T_f , is 0.01 s.

In Fig. 7, we compare the proposed estimation algorithm with the others in the autonomous valet parking scenario using the ICP method under the Welsch criterion function. The planned reference path is represented as connected-dots. If the ICP method is applied using error-free positions of the scatterers, then the actual path follows perfectly to the

reference path, which implies that the ICP method itself doesn't incur any error. With the 2D-FFT or 2D-MUSIC, the bias error accumulates and the actual path deviates from the reference path by 0.4 m at the final position, while with the LSE, the final error is about 0.2 m, which is still unacceptable for a narrow parking slot. On the other hand, the proposed algorithm gives only 0.05 m error at the final position. During the parking simulation, the total number of frames taken by the 2D-FFT, 2D-MUSIC, LSE, and proposed algorithms are 389, 401, 385, and 395, respectively.

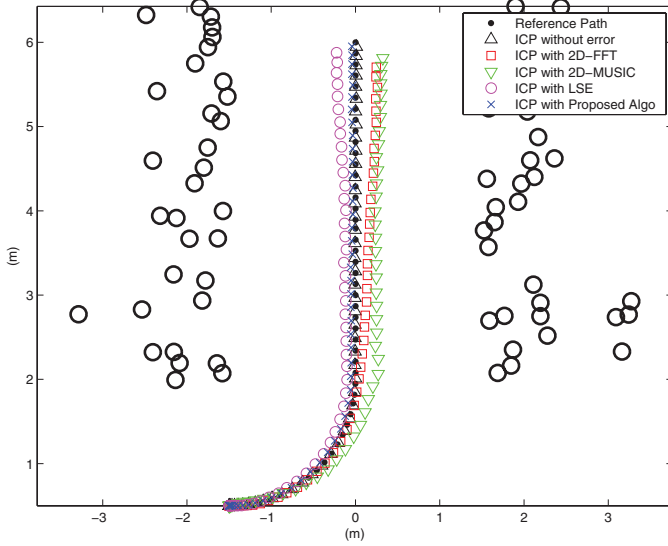


Fig. 7: The reference path and the actual paths taken by different algorithms.

VI. CONCLUSIONS

We have derived the bias error formulas in the range and angle estimates when the conventional 2D-FFT algorithm is applied on the range-angle matrix of the deramped FMCW radar signals. We have also proposed a maximum likelihood estimation algorithm that overcomes such bias error and achieves the CRB. The proposed algorithm can be used on the range-Doppler matrix or on the angle-Doppler matrix as well. We have integrated the proposed algorithm with a SLAM problem to demonstrate its applicability to high precision short-distance autonomous navigation.

APPENDIX A MLE DERIVATIONS

A.1 Parameter ψ_k

Notice that

$$\begin{aligned} \frac{\partial \Lambda}{\partial \psi_k} &= - \sum_{m=0}^{M-1} a_k \left[j e^{j(\psi_k + 2\pi \frac{u_k}{\lambda} m)} R_{(k)}^{(m)} - j e^{-j(\psi_k + 2\pi \frac{u_k}{\lambda} m)} R_{(k)}^{(m)*} \right] \\ &+ \sum_{m=0}^{M-1} \sum_{l \neq k}^K a_k a_l \left[j e^{j(\psi_k + 2\pi \frac{u_k}{\lambda} m)} e^{-j(\psi_l + 2\pi \frac{u_l}{\lambda} m)} R_{(l,k)}^{(m)} \right. \\ &\quad \left. - j e^{j(\psi_l + 2\pi \frac{u_l}{\lambda} m)} e^{-j(\psi_k + 2\pi \frac{u_k}{\lambda} m)} R_{(k,l)}^{(m)} \right] \\ &= - \sum_{m=0}^{M-1} a_k \left[j e^{j(\psi_k + 2\pi \frac{u_k}{\lambda} m)} S_{(k)}^{(m)} - j e^{-j(\psi_k + 2\pi \frac{u_k}{\lambda} m)} S_{(k)}^{(m)*} \right] \end{aligned} \quad (47)$$

$$= 2a_k \sum_{m=0}^{M-1} \text{Im} \left[e^{j\psi_k} e^{j2\pi \frac{u_k}{\lambda} m} S_{(k)}^{(m)} \right], \quad (48)$$

where

$$S_{(k)}^{(m)} = R_{(k)}^{(m)} - \sum_{l \neq k}^K a_l e^{-j(\psi_l + 2\pi \frac{u_l}{\lambda} m)} R_{(l,k)}^{(m)}. \quad (49)$$

Therefore, from $\frac{\partial \Lambda}{\partial \psi_k} = 0$, we get $\hat{\psi}_k = -\angle \left(\sum_{m=0}^{M-1} e^{j2\pi \frac{u_k}{\lambda} m} S_{(k)}^{(m)} \right)$.

A.2 Parameter a_k

Notice that

$$\begin{aligned} \frac{\partial \Lambda}{\partial a_k} &= - \sum_{m=0}^{M-1} \left[e^{j(\psi_k + 2\pi \frac{u_k}{\lambda} m)} R_{(k)}^{(m)} + e^{-j(\psi_k + 2\pi \frac{u_k}{\lambda} m)} R_{(k)}^{(m)*} \right] \\ &+ \sum_{m=0}^{M-1} \sum_{l \neq k}^K a_l \left[e^{j(\psi_k + 2\pi \frac{u_k}{\lambda} m)} e^{-j(\psi_l + 2\pi \frac{u_l}{\lambda} m)} R_{(l,k)}^{(m)} \right. \\ &\quad \left. + e^{j(\psi_l + 2\pi \frac{u_l}{\lambda} m)} e^{-j(\psi_k + 2\pi \frac{u_k}{\lambda} m)} R_{(k,l)}^{(m)} \right] \\ &+ 2MN a_k \\ &= -2 \sum_{m=0}^{M-1} \text{Re} \left[e^{j(\psi_k + 2\pi \frac{u_k}{\lambda} m)} R_{(k)}^{(m)} \right] \\ &+ 2 \sum_{m=0}^{M-1} \sum_{l \neq k}^K a_l \text{Re} \left[e^{j(\psi_k + 2\pi \frac{u_k}{\lambda} m)} e^{-j(\psi_l + 2\pi \frac{u_l}{\lambda} m)} R_{(l,k)}^{(m)} \right] \\ &+ 2MN a_k. \end{aligned} \quad (50)$$

Therefore, from $\frac{\partial \Lambda}{\partial a_k} = 0$, we get

$$\begin{aligned} \hat{a}_k &= \frac{1}{MN} \left[\sum_{m=0}^{M-1} \text{Re} \left[e^{j(\psi_k + 2\pi \frac{u_k}{\lambda} m)} R_{(k)}^{(m)} \right] \right. \\ &\quad \left. - \sum_{m=0}^{M-1} \sum_{l \neq k}^K a_l \text{Re} \left[e^{j(\psi_k + 2\pi \frac{u_k}{\lambda} m)} e^{-j(\psi_l + 2\pi \frac{u_l}{\lambda} m)} R_{(l,k)}^{(m)} \right] \right]. \end{aligned} \quad (52)$$

The matrix form of this equation is (37).

A.3 Parameter u_k

Jacobian of $\Lambda(\cdot)$ with respect to u_k is as follows.

$$\begin{aligned} f_u &= \frac{\partial \Lambda}{\partial u_k} = -a_k \sum_{m=0}^{M-1} \left[j \frac{2\pi}{\lambda} m e^{j(\psi_k + 2\pi \frac{u_k}{\lambda} m)} R_{(k)}^{(m)} \right. \\ &\quad \left. - j \frac{2\pi}{\lambda} m e^{-j(\psi_k + 2\pi \frac{u_k}{\lambda} m)} R_{(k)}^{(m)*} \right. \\ &\quad \left. + e^{j(\psi_k + 2\pi \frac{u_k}{\lambda} m)} \frac{\partial R_{(k)}^{(m)}}{\partial u_k} + e^{-j(\psi_k + 2\pi \frac{u_k}{\lambda} m)} \frac{\partial R_{(k)}^{(m)*}}{\partial u_k} \right] \\ &+ a_k \sum_{m=0}^{M-1} \sum_{l \neq k}^K \left[a_l \left(j \frac{2\pi}{\lambda} m \right) e^{j(\psi_k + 2\pi \frac{u_k}{\lambda} m)} e^{-j(\psi_l + 2\pi \frac{u_l}{\lambda} m)} R_{(l,k)}^{(m)} \right. \\ &\quad \left. + a_l e^{j(\psi_k + 2\pi \frac{u_k}{\lambda} m)} e^{-j(\psi_l + 2\pi \frac{u_l}{\lambda} m)} \frac{\partial R_{(l,k)}^{(m)}}{\partial u_k} \right. \\ &\quad \left. + a_l \left(-j \frac{2\pi}{\lambda} m \right) e^{-j(\psi_k + 2\pi \frac{u_k}{\lambda} m)} e^{j(\psi_l + 2\pi \frac{u_l}{\lambda} m)} R_{(l,k)}^{(m)*} \right. \\ &\quad \left. + a_l e^{-j(\psi_k + 2\pi \frac{u_k}{\lambda} m)} e^{j(\psi_l + 2\pi \frac{u_l}{\lambda} m)} \frac{\partial R_{(l,k)}^{(m)*}}{\partial u_k} \right] \end{aligned} \quad (53)$$

$$\begin{aligned}
&= \frac{4\pi}{\lambda} a_k \sum_{m=0}^{M-1} m \text{Im}[e^{j(\psi_k + 2\pi \frac{u_k}{\lambda} m)} R_{(k)}^{(m)}] \\
&\quad - 2a_k \sum_{m=0}^{M-1} \text{Re}[e^{j(\psi_k + 2\pi \frac{u_k}{\lambda} m)} \frac{\partial R_{(k)}^{(m)}}{\partial u_k}] \\
&\quad - \frac{4\pi}{\lambda} a_k \sum_{m=0}^{M-1} \sum_{l \neq k}^K m \text{Im}[e^{j(\psi_k + 2\pi \frac{u_k}{\lambda} m)} a_l e^{-j(\psi_l + 2\pi \frac{u_l}{\lambda} m)} R_{(l,k)}^{(m)}] \\
&\quad + 2a_k \sum_{m=0}^{M-1} \sum_{l \neq k}^K a_l \text{Re}[e^{j(\psi_k + 2\pi \frac{u_k}{\lambda} m)} e^{-j(\psi_l + 2\pi \frac{u_l}{\lambda} m)} \frac{\partial R_{(l,k)}^{(m)}}{\partial u_k}]
\end{aligned} \tag{54}$$

$$\begin{aligned}
&= \frac{4\pi}{\lambda} a_k \sum_{m=0}^{M-1} m \text{Im}[e^{j(\psi_k + 2\pi \frac{u_k}{\lambda} m)} S_{(k)}^{(m)}] \\
&\quad - 2a_k \sum_{m=0}^{M-1} \text{Re}[e^{j(\psi_k + 2\pi \frac{u_k}{\lambda} m)} \frac{\partial S_{(k)}^{(m)}}{\partial u_k}],
\end{aligned} \tag{55}$$

where

$$\frac{\partial S_{(k)}^{(m)}}{\partial u_k} = \frac{\partial R_{(k)}^{(m)}}{\partial u_k} - \sum_{l \neq k}^K a_l e^{-j(\psi_l + 2\pi \frac{u_l}{\lambda} m)} \frac{\partial R_{(l,k)}^{(m)}}{\partial u_k}, \tag{56}$$

$$\frac{\partial R_{(k)}^{(m)}}{\partial u_k} = \sum_{n=0}^{N-1} z^*[n, m] \left[j \frac{2\pi B}{cN} mn \right] e^{j2\pi(2r_k + mu_k) \frac{B}{cN} n}, \tag{57}$$

$$\frac{\partial R_{(l,k)}^{(m)}}{\partial u_k} = \sum_{n=0}^{N-1} \left[j \frac{2\pi B}{cN} mn \right] e^{j2\pi(2(r_k - r_l) + m(u_k - u_l)) \frac{B}{cN} n}. \tag{58}$$

The Hessian of $\Lambda(\cdot)$ with respect to u_k is given by

$$\begin{aligned}
f'_u &= \frac{\partial}{\partial u_k} \left(\frac{\partial \Lambda}{\partial u_k} \right) = \frac{4\pi}{\lambda} a_k \sum_{m=0}^{M-1} m \frac{\partial}{\partial u_k} \text{Im}[e^{j(\psi_k + 2\pi \frac{u_k}{\lambda} m)} S_{(k)}^{(m)}] \\
&\quad - 2a_k \sum_{m=0}^{M-1} \frac{\partial}{\partial u_k} \text{Re}[e^{j(\psi_k + 2\pi \frac{u_k}{\lambda} m)} \frac{\partial S_{(k)}^{(m)}}{\partial u_k}] \\
&= 2 \left(\frac{2\pi}{\lambda} \right)^2 a_k \sum_{m=0}^{M-1} m^2 \text{Re}[e^{j(\psi_k + 2\pi \frac{u_k}{\lambda} m)} S_{(k)}^{(m)}] \\
&\quad + 4 \left(\frac{2\pi}{\lambda} \right) a_k \sum_{m=0}^{M-1} m \text{Im}[e^{j(\psi_k + 2\pi \frac{u_k}{\lambda} m)} \frac{\partial S_{(k)}^{(m)}}{\partial u_k}] \\
&\quad - 2a_k \sum_{m=0}^{M-1} \text{Re} \left[e^{j(\psi_k + 2\pi \frac{u_k}{\lambda} m)} \frac{\partial^2 S_{(k)}^{(m)}}{\partial u_k^2} \right],
\end{aligned} \tag{59}$$

where

$$\frac{\partial^2 S_{(k)}^{(m)}}{\partial u_k^2} = \frac{\partial^2 R_{(k)}^{(m)}}{\partial u_k^2} - \sum_{l \neq k}^K a_l e^{-j(\psi_l + 2\pi \frac{u_l}{\lambda} m)} \frac{\partial^2 R_{(l,k)}^{(m)}}{\partial u_k^2}, \tag{61}$$

$$\frac{\partial^2 R_{(k)}^{(m)}}{\partial u_k^2} = - \sum_{n=0}^{N-1} z^*[n, m] \left(\frac{2\pi B}{cN} mn \right)^2 e^{j2\pi(2r_k + mu_k) \frac{B}{cN} n}, \tag{62}$$

$$\frac{\partial^2 R_{(l,k)}^{(m)}}{\partial u_k^2} = - \sum_{n=0}^{N-1} \left(\frac{2\pi B}{cN} mn \right)^2 e^{j2\pi(2(r_k - r_l) + m(u_k - u_l)) \frac{B}{cN} n}. \tag{63}$$

We note that

$$\begin{aligned}
\frac{\partial}{\partial u_k} \text{Im}[e^{j(\psi_k + 2\pi \frac{u_k}{\lambda} m)} S_{(k)}^{(m)}] &= \frac{2\pi}{\lambda} m \text{Re}[e^{j(\psi_k + 2\pi \frac{u_k}{\lambda} m)} S_{(k)}^{(m)}] \\
&\quad + \text{Im}[e^{j(\psi_k + 2\pi \frac{u_k}{\lambda} m)} \frac{\partial S_{(k)}^{(m)}}{\partial u_k}],
\end{aligned} \tag{64}$$

$$\begin{aligned}
&\frac{\partial}{\partial u_k} \text{Re}[e^{j(\psi_k + 2\pi \frac{u_k}{\lambda} m)} \frac{\partial S_{(k)}^{(m)}}{\partial u_k}] = \\
&\quad - \frac{2\pi}{\lambda} m \text{Im}[e^{j(\psi_k + 2\pi \frac{u_k}{\lambda} m)} \frac{\partial S_{(k)}^{(m)}}{\partial u_k}] + \text{Re}[e^{j(\psi_k + 2\pi \frac{u_k}{\lambda} m)} \frac{\partial^2 S_{(k)}^{(m)}}{\partial u_k^2}].
\end{aligned} \tag{65}$$

A.4 Parameter r_k

Jacobian of $\Lambda(\cdot)$ with respect to r_k is as follows.

$$\begin{aligned}
f_r &= \frac{\partial \Lambda}{\partial r_k} = - \sum_{m=0}^{M-1} \left[a_k e^{j(\psi_k + 2\pi \frac{u_k}{\lambda} m)} \frac{\partial R_{(k)}^{(m)}}{\partial r_k} \right. \\
&\quad \left. + a_k e^{-j(\psi_k + 2\pi \frac{u_k}{\lambda} m)} \frac{\partial R_{(k)}^{(m)*}}{\partial r_k} \right] \\
&\quad + \sum_{m=0}^{M-1} \sum_{l \neq k}^K \left[a_k a_l e^{j(\psi_k + 2\pi \frac{u_k}{\lambda} m)} e^{-j(\psi_l + 2\pi \frac{u_l}{\lambda} m)} \frac{\partial R_{(l,k)}^{(m)}}{\partial r_k} \right. \\
&\quad \left. + a_k a_l e^{-j(\psi_k + 2\pi \frac{u_k}{\lambda} m)} e^{j(\psi_l + 2\pi \frac{u_l}{\lambda} m)} \frac{\partial R_{(l,k)}^{(m)*}}{\partial r_k} \right]
\end{aligned} \tag{66}$$

$$= -2a_k \sum_{m=0}^{M-1} \text{Re}[e^{j(\psi_k + 2\pi \frac{u_k}{\lambda} m)} \frac{\partial S_{(k)}^{(m)}}{\partial r_k}], \tag{67}$$

where

$$\frac{\partial S_{(k)}^{(m)}}{\partial r_k} = \frac{\partial R_{(k)}^{(m)}}{\partial r_k} - \sum_{l \neq k}^K a_l e^{-j(\psi_l + 2\pi \frac{u_l}{\lambda} m)} \frac{\partial R_{(l,k)}^{(m)}}{\partial r_k}, \tag{68}$$

$$\frac{\partial R_{(k)}^{(m)}}{\partial r_k} = \sum_{n=0}^{N-1} z^*[n, m] \left[j \frac{4\pi B}{cN} n \right] e^{j2\pi(2r_k + mu_k) \frac{B}{cN} n}, \tag{69}$$

$$\frac{\partial R_{(l,k)}^{(m)}}{\partial r_k} = \sum_{n=0}^{N-1} \left[j \frac{4\pi B}{cN} n \right] e^{j2\pi(2(r_k - r_l) + m(u_k - u_l)) \frac{B}{cN} n}. \tag{70}$$

The Hessian of $\Lambda(\cdot)$ with respect to r_k is given by

$$f'_r = \frac{\partial}{\partial r_k} \left(\frac{\partial \Lambda}{\partial r_k} \right) = -2a_k \sum_{m=0}^{M-1} \text{Re} \left[e^{j(\psi_k + 2\pi \frac{u_k}{\lambda} m)} \frac{\partial^2 S_{(k)}^{(m)}}{\partial r_k^2} \right], \tag{71}$$

where

$$\frac{\partial^2 S_{(k)}^{(m)}}{\partial r_k^2} = \frac{\partial^2 R_{(k)}^{(m)}}{\partial r_k^2} - \sum_{l \neq k}^K a_l e^{-j(\psi_l + 2\pi \frac{u_l}{\lambda} m)} \frac{\partial^2 R_{(l,k)}^{(m)}}{\partial r_k^2}, \tag{72}$$

$$\frac{\partial^2 R_{(k)}^{(m)}}{\partial r_k^2} = - \sum_{n=0}^{N-1} z^*[n, m] \left[\frac{4\pi B}{cN} n \right]^2 e^{j2\pi(2r_k + mu_k) \frac{B}{cN} n}, \tag{73}$$

$$\frac{\partial^2 R_{(l,k)}^{(m)}}{\partial r_k^2} = - \sum_{n=0}^{N-1} \left[\frac{4\pi B}{cN} n \right]^2 e^{j2\pi(2(r_k - r_l) + m(u_k - u_l)) \frac{B}{cN} n}. \tag{74}$$

APPENDIX B CRAMER-RAO BOUNDS

Let $\boldsymbol{\omega} = [\omega_1, \omega_2, \omega_3, \omega_4]^T = [a, \psi, r, u]^T$. Then the covariance matrix $\mathbf{C}_{\hat{\boldsymbol{\omega}}} \in \mathbb{R}^{4 \times 4}$ of an unbiased estimator $\hat{\boldsymbol{\omega}}$ has the lower bound $\mathbf{C}_{\hat{\boldsymbol{\omega}}} \geq \mathbf{I}^{-1}(\boldsymbol{\omega})$. For our measurement model,

$$z[n, m] = s[n, m] + w[n, m], \tag{75}$$

where $s[n, m] = ae^{j(\psi + 2\pi \frac{u}{\lambda} m + 2\pi(2r + mu) \frac{B}{cN} n)}$, and $\mathbf{I}(\omega)$ is given by

$$[\mathbf{I}(\omega)]_{i,j} = \frac{2}{\sigma^2} \sum_{m=0}^{M-1} \sum_{n=0}^{N-1} \left[\frac{\partial \mu[n, m]}{\partial \omega_i} \frac{\partial \mu[n, m]}{\partial \omega_j} + \frac{\partial \nu[n, m]}{\partial \omega_i} \frac{\partial \nu[n, m]}{\partial \omega_j} \right], \quad (76)$$

where $\mu[n, m] = \text{Re}[s[n, m]]$ and $\nu[n, m] = \text{Im}[s[n, m]]$. Therefore, with the definition, $h[n, m] = \psi + 2\pi \frac{u}{\lambda} m + 2\pi(2r + mu) \frac{B}{cN} n$, we get

$$\frac{\partial \mu[n, m]}{\partial \omega_1} = \cos(h[n, m]), \quad \frac{\partial \mu[n, m]}{\partial \omega_2} = -a \sin(h[n, m]), \quad (77)$$

$$\frac{\partial \mu[n, m]}{\partial \omega_3} = -4\pi a \frac{B}{cN} n \sin(h[n, m]), \quad (78)$$

$$\frac{\partial \mu[n, m]}{\partial \omega_4} = -2\pi am \left(\frac{1}{\lambda} + \frac{B}{cN} n \right) \sin(h[n, m]), \quad (79)$$

$$\frac{\partial \nu[n, m]}{\partial \omega_1} = \sin(h[n, m]), \quad \frac{\partial \nu[n, m]}{\partial \omega_2} = a \cos(h[n, m]), \quad (80)$$

$$\frac{\partial \nu[n, m]}{\partial \omega_3} = 4\pi a \frac{B}{cN} n \cos(h[n, m]), \quad (81)$$

$$\frac{\partial \nu[n, m]}{\partial \omega_4} = 2\pi am \left(\frac{1}{\lambda} + \frac{B}{cN} n \right) \cos(h[n, m]). \quad (82)$$

Therefore,

$$\mathbf{I}(\omega) = \frac{2}{\sigma^2} \sum_{m=0}^{M-1} \sum_{n=0}^{N-1} \begin{bmatrix} 1 & 0 & 0 & 0 \\ 0 & a^2 & 4\pi a^2 \frac{B}{cN} n & i_{2,4} \\ 0 & 4\pi a^2 \frac{B}{cN} n & i_{3,3} & i_{3,4} \\ 0 & i_{4,2} & i_{4,3} & i_{4,4} \end{bmatrix}, \quad (83)$$

where

$$i_{2,4} = i_{4,2} = 2\pi a^2 m \left[\frac{1}{\lambda} + \frac{B}{cN} n \right], \quad i_{3,3} = \left[4\pi a \frac{B}{cN} n \right]^2, \quad (84)$$

$$i_{3,4} = i_{4,3} = 2(2\pi a)^2 \left[\frac{1}{\lambda} + \frac{B}{cN} n \right] \frac{B}{cN} mn, \quad (85)$$

$$i_{4,4} = (2\pi am)^2 \left[\frac{1}{\lambda} + \frac{B}{cN} n \right]^2. \quad (86)$$

We can easily find the 3rd and 4th diagonal entries of $\mathbf{I}^{-1}(\omega)$, using the Cramer's rule to get the CRB of r and θ ;

$$\sigma_{r,CRB} = \sqrt{[\mathbf{I}^{-1}(\omega)]_{3,3}} \quad (87)$$

$$\sigma_{\theta,CRB} = \sqrt{[\mathbf{I}^{-1}(\omega)]_{4,4}} \frac{du}{d\theta} = \sqrt{[\mathbf{I}^{-1}(\omega)]_{4,4}} / (d \cos \theta). \quad (88)$$

where $u = d \sin \theta$, and the unit of $\sigma_{\theta,CRB}$ is radian.

REFERENCES

- [1] M. I. Skolnik, "Introduction to radar," *Radar Handbook*, vol. 2, 1962.
- [2] J. Hasch, E. Topak, R. Schnabel, T. Zwick, R. Weigel, and C. Waldschmidt, "Millimeter-wave technology for automotive radar sensors in the 77 GHz frequency band," *IEEE Transactions on Microwave Theory and Techniques*, vol. 60, no. 3 PART 2, pp. 845–860, Mar 2012.
- [3] H. Rohling and M.-M. Meinecke, "Waveform design principles for automotive radar systems," in *CIE International Conference on Radar, Proceedings*, vol. 1, Beijing, China, 2001, pp. 1–4.
- [4] M. Schneider, "Automotive radar—status and trends," in *German microwave conference, GeMiC 2005*, Munich, Germany, 2005, pp. 144–147.
- [5] A. Meta, P. Hooeboom, and L. P. Ligthart, "Signal processing for FMCW SAR," *IEEE Transactions on Geoscience and Remote Sensing*, vol. 45, no. 11, pp. 3519–3532, Nov 2007.
- [6] R. Wang, Y. H. Luo, Y. K. Deng, Z. M. Zhang, and Y. Liu, "Motion compensation for high-resolution automobile FMCW SAR," *IEEE Geoscience and Remote Sensing Letters*, vol. 10, no. 5, pp. 1157–1161, Sep 2013.
- [7] R. Wang, O. Loffeld, H. Nies, S. Knedlik, M. Hägelen, and H. Essen, "Focus FMCW SAR data using the wavenumber domain algorithm," *IEEE Transactions on Geoscience and Remote Sensing*, vol. 48, no. 4 PART 2, pp. 2109–2118, Apr 2010.
- [8] E. Giusti and M. Martorella, "Range doppler and image autofocusing for FMCW inverse synthetic aperture radar," *IEEE Transactions on Aerospace and Electronic Systems*, vol. 47, no. 4, pp. 2807–2823, Oct 2011.
- [9] Y. Liu, Y. K. Deng, R. Wang, and O. Loffeld, "Bistatic FMCW SAR signal model and imaging approach," *IEEE Transactions on Aerospace and Electronic Systems*, vol. 49, no. 3, pp. 2017–2028, Jul 2013.
- [10] A. G. Stove, "Linear FMCW radar techniques," in *IEE Proceedings F-Radar and Signal Processing*, vol. 139, no. 5. IET, Oct 1992, pp. 343–350.
- [11] P. Brennan, Y. Huang, M. Ash, and K. Chetty, "Determination of sweep linearity requirements in fmcw radar systems based on simple voltage-controlled oscillator sources," *IEEE Transactions on Aerospace and Electronic Systems*, vol. 47, no. 3, pp. 1594–1604, Jul 2011.
- [12] G. Babur, O. A. Krasnov, A. Yarovoy, and P. Aubry, "Nearly orthogonal waveforms for MIMO FMCW radar," *IEEE Transactions on Aerospace and Electronic Systems*, vol. 49, no. 3, pp. 1426–1437, Jul 2013.
- [13] R. Feger, C. Wagner, S. Schuster, S. Scheibhofer, H. Jager, and A. Stelzer, "A 77-GHz FMCW MIMO radar based on an SiGe single-chip transceiver," *IEEE Transactions on Microwave Theory and Techniques*, vol. 57, no. 5, pp. 1020–1035, May 2009.
- [14] F. Belfiori, W. van Rossum, and P. Hooeboom, "2D-MUSIC technique applied to a coherent FMCW MIMO radar," in *Radar Systems (Radar 2012), IET International Conference on*, Glasgow, United Kingdom, Oct 2012, pp. 1–6.
- [15] U. Majumder, M. R. Bell, and M. Rangaswamy, "Design and analysis of radar waveforms achieving transmit and receive orthogonality," *IEEE Transactions on Aerospace and Electronic Systems*, vol. 52, no. 3, pp. 1056–1066, Jun 2016.
- [16] A. N. Lemma, A. J. Van Der Veen, and E. F. Deprettere, "Analysis of joint angle-frequency estimation using ESPRIT," *IEEE Transactions on Signal Processing*, vol. 51, no. 5, pp. 1264–1283, May 2003.
- [17] S. Kim, D. Oh, and J. Lee, "Joint DFT-ESPRIT Estimation for TOA and DOA in Vehicle FMCW Radars," *IEEE Antennas and Wireless Propagation Letters*, vol. 14, pp. 1710–1713, Apr 2015.
- [18] R. Feger, S. Schuster, S. Scheibhofer, and A. Stelzer, "Sparse antenna array design and combined range and angle estimation for FMCW radar sensors," in *2008 IEEE Radar Conference, RADAR 2008*, Rome, Italy, May 2008, pp. 1–6.
- [19] O. Saleh, M. Raven, R. Riddolls, and R. Adve, "Fast fully adaptive processing: a multistage stap approach," *IEEE Transactions on Aerospace and Electronic Systems*, vol. 52, no. 5, pp. 2168–2183, Oct 2016.
- [20] M. Adams, J. Mullane, E. Jose, and B.-N. Vo, *Robotic Navigation and Mapping with Radar*. Boston: Artech House, 2012.
- [21] H. Lee, J. Chun, K. Jeon, and H. Lee, "Efficient EKF-SLAM algorithm based on measurement clustering and real data simulation," in *IEEE 88th Vehicular Technology Conference - Fall*, Chicago, USA, Aug 2018.
- [22] P.-J. Nordlund and F. Gustafsson, "Marginalized particle filter for accurate and reliable terrain-aided navigation," *IEEE Transactions on Aerospace and Electronic Systems*, vol. 45, no. 4, pp. 1385–1399, Oct 2009.
- [23] I. E. Paromtchik and C. Laugier, "Motion generation and control for parking an autonomous vehicle," in *Robotics and Automation, 1996. Proceedings., 1996 IEEE International Conference on*, vol. 4, Minneapolis, Minnesota, USA, Apr 1996, pp. 3117–3122.
- [24] I. E. Paromtchik and Laugier, "Autonomous parallel parking of a nonholonomic vehicle," in *Intelligent Vehicles Symposium, 1996., Proceedings of the 1996 IEEE*, Paris, France, Oct 1996, pp. 13–18.
- [25] T. H. Hsu, J. F. Liu, P. N. Yu, W. S. Lee, and J. S. Hsu, "Development of an automatic parking system for vehicle," in *2008 IEEE Vehicle Power and Propulsion Conference, VPPC 2008*, Harbin, China, Sep 2008, pp. 1–6.
- [26] P. Besl and N. McKay, "A Method for Registration of 3-D Shapes," *IEEE Transactions on Pattern Analysis and Machine Intelligence*, vol. 14, no. 2, pp. 239–256, Feb 1992.